FABRICATION OF SOLID POLYMERIC 3D SHAPES FROM PROGRAMMABLE FLAT

HYDROGEL SHEETS

by

NINAD VILAS KHADSE

Presented to the Faculty of the Graduate School of

The University of Texas at Arlington in Partial Fulfillment

of the Requirements

for the Degree of

MASTER OF SCIENCE IN MATERIALS SCIENCE AND ENGINEERING

THE UNIVERSITY OF TEXAS AT ARLINGTON

MAY 2018

Acknowledgments

I want to thank Dr. Kyungsuk Yum for the guidance towards this thesis and support throughout my time working with his research group.

I wish to offer thanks to Dr. Efstathios Meletis's, chair of MSE department, and Dr. Seong Jin Koh, graduate advisor of MSE department for their kind support.

I am also grateful for the help from my colleagues Mr. Amirali Nojoomi, Hakan Arslan and Mr. Sunil Yadav.

My special thanks are extended towards my parents, family and friends who have always supported me through highs and lows.

May 8, 2018

Abstract

FABRICATION OF SOLID POLYMERIC 3D SHAPES FROM PROGRAMMABLE FLAT

HYDROGEL SHEETS

Ninad Vilas Khadse, MS

The University of Texas at Arlington, 2018

Supervising Professor: Kyungsuk Yum

Modern methods of fabricating three-dimensional (3D) objects include sheet metal forming, thermoforming, and additive manufacturing among others. These methods have their own advantages and disadvantages regarding scalability, customizability, and time efficiency. A promising approach is to program the growth (expansion and contraction) of hydrogel sheets to form 3D structures. The differential growth-induced 3D shaping approach has the advantages of traditional manufacturing (scalability) and additive manufacturing (customizability). The objective of this study is to create nanocomposite 3D structures that are stable in ambient environment using the growth-induced 3D shaping approach. This study determines the effect of silica nanoparticles in hydrogels on the shape forming capability to build 3D structures of silica nanocomposites. The drying process of nanocomposite hydrogels at the shrunk state leads to air-stable 3D structures. The mechanical properties of the resulting 3D structures are comparable to those of polymer structures fabricated by conventional additive manufacturing methods. The hardness and yield strength of the structures increase with the concentration of silica nanoparticles in them. Scanning electron microscopy shows an excellent surface finish of the fabricated 3D structures. This approach could open new routes for manufacturing 3D structures with customized design in a scalable way.

Table of Contents

List of Illustrations

List of Tables

Chapter 1

Overview

1.1 Overview

Additive Manufacturing, Rapid Prototyping, Solid Freeform Fabrication or 3D Printing are terms used to describe the process of joining together layers with the help of a computer to build up a 3D object. The object to be printed is built up from multiple superimposed 2D layers which are stuck to each other depending on the specific apparatus and technique used as opposed to subtractive manufacturing where an object is made by successive removal of material by milling, cutting much of which is done on Computer Numerical Control (CNC) machines today. This process of designing and printing the object takes place in significantly less time as compared to conventional methods and also reduces the cost of fabrication.

Scaffolds for bone growth have been fabricated using Stereolithography as the scaffold porosity can be better controlled and biocompatible materials can also be used in this process which provides a capability for customization of the scaffold[1]. Advances in this field have reached a level such that more than a third of the components of a turbo engine for aircraft is being built using 3D printing by General Electric[2]. The major bottlenecks in making 3D printing a truly commercial process are the huge printing times, the need for post-processing, limited scalability and the presence of supports. 4D printing is turning out to be a technique which could address most of these problems. Fabrication time could be reduced to minutes while being able to print appreciable large structures which change as a response to stimuli.

Sheet forming is a method used in industry to produce multiple objects in a single step using specific molds for a particular shape. Although this method is good for mass production, it lacks the versatility and customizability of 3D printing. Moreover, these

machines are bulky and not portable which means they have a high setup cost. This process is highly scalable as multiple components can be stamped or pressed at the same time in a large enough sheet of metal but lacks the customizability of 3D printing.

The advantages of 3D printing and sheet forming methods can be combined by using 4D printing of hydrogels. In this study, we describe an established method for 4D printing and study the same to obtain dried nanocomposites which combine the advantages of 3D printing and sheet forming. We use a DLP based 3D printed to project grayscale masks on a precursor layer to fabricate flat sheets with varying crosslinks which is used to program a required shape. These sheets are then swelled in water and then deswelled above to obtain the programmed shape. We calibrate this system for ceramic nanoparticle-based precursors, after which we print some principle shapes to determine the accuracy which are then dried with an emphasis on accurately retaining the desired curvatures.

1.2 Thesis Outline

The objectives of this thesis are to:

1) Study the effect of nanoparticle loading on shape forming behavior and compare with pure polymeric precursor
2) To fabricate principle shapes and determine the printing accuracy
3) To establish a process to stabilize the deswelled shapes in air
4) To evaluate physical, mechanical and system dependent properties of the solid shapes

The thesis is organized as follows:

Chapter 2 introduces 3D printing, 4D printing and nanocomposite fabrication using 3D printing. Techniques of 4D printing and the mechanisms therein are also discussed.

Chapter 3 talks about the background for this study which includes the basic idea behind our system. The thermosensitive polymer used in this study is also discussed along with previous studies based on this polymer.

Chapter 4 describes the experimental part of the study. The objectives are mentioned and results to achieve the same are shown using gathered data.

Chapter 5 contains discussion about the study.

Chapter 6 concludes the study by stating the outcomes and finally summarizing the study.

Chapter 2

Introduction

2.1 3D Printing

2.1.1 Fused Deposition Modelling

Fused Deposition Modelling (FDM) is the most important 3D printing and has popularized and proved the importance of 3D printing in the rapid prototyping space[3]. FDM printing works on the simple principle of extruding a hot viscous plastic from an extrusion print head/nozzle over a bed/platform which solidifies to form a layer which is written over by another layer by the plastic flowing through the nozzle. The nozzle has heaters on it which het up the nozzle and subsequently the filament at the tip of the nozzle flows as the temperature reaches above the melting temperature for semi-crystalline polymers and above the glass transition temperature for amorphous polymers. The polymer solidifies on the bed as its temperature drops below the melting or glass transition temperature.

Filament

Extrusion Print Head -----

Heated Nozzle -----------

3D Model -----

Build Platform
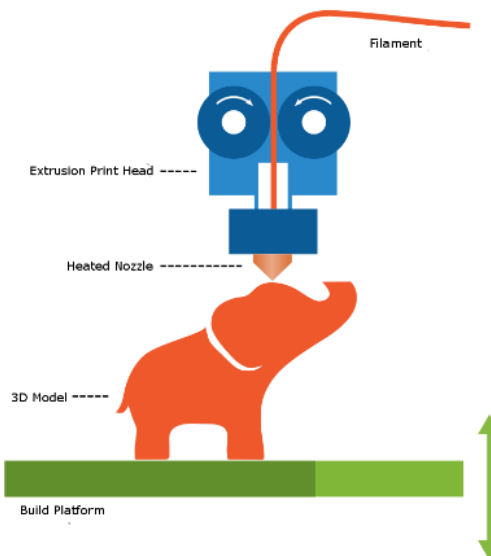
Figure 2-1 Fused Deposition Modeling diagram

The nozzle moves in the X-Y plane following a certain path specified by the information from a slicing software. After a layer is printed and solidified, either the bed moves down

4

or the print head moves up in the Z-direction so that the next layer can be printed on top of the previous. This process continues till the complete model is printed to form a 3D object and then the object is detached from the bed. Post-processing operations such as support removal, sanding, cold welding, polishing or painting is done at the end.

2.1.2 Stereolithography/Digital Light Processing

Stereolithography (SLA) is a process of forming solid objects from a resin by using light for the act of solidification/crosslinking. A coherent source of light, usually a laser operating in the UV range is used for inducing crosslinking. The laser spot size is incredibly small which means that the resolution of printing in the X-Y plane is very high. The laser pointer is scanned onto the surface by a scanner system which usually consists of two mirrors which can tilt and guide the laser to change its position for printing.
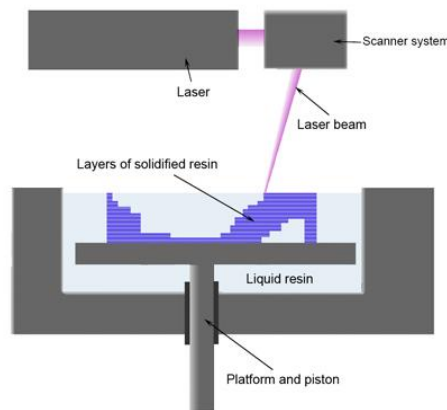
Figure 2-2 Stereolithography schematic diagram

The printer consists of a vat containing the resin, the platform onto which the model is printed and the sweeper. After the printer receives the printing instructions, the scanner system and the laser work to print the first layer after which the vat shifts downwards by a distance equal to the layer height and the sweeper coats the previously printed layer with fresh resin and a new layer is printed by the laser. This process continues until all the layers have been printed after which the object is detached from the platform and the excess resin from its surface is cleaned off.

Digital Light Processing (DLP) printing is similar to SLA except that the vat has a transparent bottom surface and instead of a laser and scanner system, it utilized a DLP projector which projects the complete image of a layer from beneath the vat such that the resin solidifies on the platform. The platform moves up by a distance equal to the specified layer height and the sweeper coats fresh resin for the next layer. This process uses pixels to print a layer which consists of multiple voxels (volumetric pixels) whose height depends on the layer thickness.
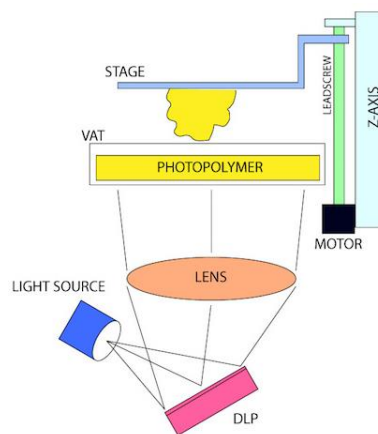
Figure 2-3 DLP Printing diagram

Both these techniques are used for fabricating objects requiring intricate detail reproduction. The DLP build time is significantly less as the whole layer is printed in a single step as opposed to SLA where the laser has to be scanned across the surface to print the layer. Objects fabricated using SLA or DLP printing are usually fragile when compared to counterparts formed using industrial processes like injection molding.

Resins used in SLA and DLP printing are photocurable meaning that photoinitiators are an integral part which formulating a resin. One of the earliest patents for a photocurable resin describes the monomer to be a "resinous polyacrylate or polymethacrylate" dissolved in "liquid polyacrylate or polymethacrylate" and "liquid N-vinyl monomer, preferably N-vinyl

pyrrolidone"[4]. Another patent describes the use of an urethane acrylate monomer along with an acrylate monomer in the resin[5].

2.1.3 Selective Laser Sintering

Selective Laser Sintering (SLS) is a technique which is based on powder sintering and solidification. This is achieved by using a high-power laser capable of heating up a suitable powder which absorbs the generated heat such that the particles bind together. The powder is spread on the powder bed by a roller or a blade after which the laser scans and solidifies the first layer based on the layer data. The roller then spreads a new layer of powder on the previously created layer which is then again scanned by the laser and the next layer is printed on top of the first layer. The cross-sections of the object are printed layer by layer to form a 3D object.
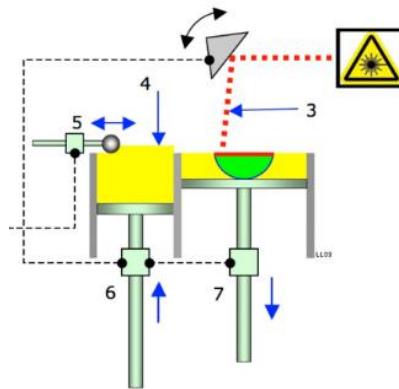
Figure 2-4 Selective Laser Sintering schematic diagram[6]

The object to be printed is designed in a CAD software followed by a slicing software which slices the object into layers to be printed. After the information is fed to the printed, the roller lays out the first layer of powder on the bed and the laser scans the powder and then proceeds to print the first layer by selectively solidifying the powder and a piston lowers the bed. A separate piston pushes the powder reservoir upwards and the roller lays out another

layer of powder which gets solidified as the second layer. While printing the bed and powder is maintained at a suitable elevated temperature which is just a few degrees below the softening temperature of the powder. This is done to decrease the amount of processing time and also to minimize thermally induced stresses which can develop during cooling of the layers.

Supporting structures are not needed in this technique as the unsintered powder holds the sintered layers in place. Smaller particle size results in higher resolution and lower surface roughness. To improve this property, bimodal powders are used which also help improve flowability. Sintering using lasers takes a very short interval of a few milliseconds which is not enough for the particles to sufficiently sinter together. The powders are made of a low melting and high melting components such that the low melting components melt immediately due to the heat from the laser and bind the high melting powders.

2.2 4D Printing

2.2.1 Overview

The advent of 3D printing gave way to an impressive amount of scientific research in the field but with a saturation in possible fabrication techniques and increased interest in the printing time aspect of the process, the field of 4d printing opened up and is expected to see a huge growth in the years to come. The 4th dimension here is considered to be time which is used to trigger a shape change in the 3D printed part after the printing process. Thus, a dynamic object is fabricated which changes shape with an external trigger or stimuli. The printed objects can be programmed to a certain shape or multiple shapes and can cycle between these based on a suitable trigger or stimuli according to the system used. Environment-responsive tires could provide better traction by changing shape. Clothing and shoes could be manufactured which change their shape to provide a perfect fit to the wearer. A major advantage of 4D printed parts is that they would be able to adapt

and shape themselves around structures around them based on changes in the environment because of their dynamic nature.
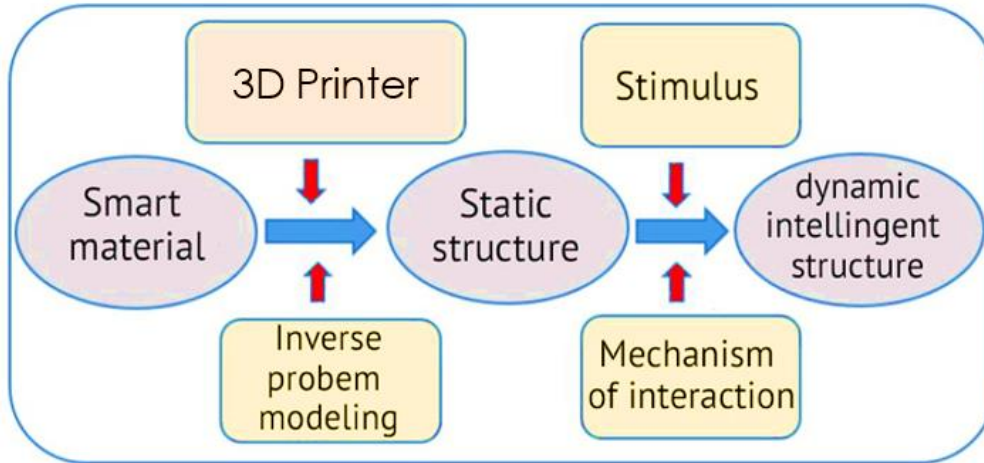
Figure 2-5 4D printing schematic

4D printing is already being explored to replace sensitive hardware. Airbus is developing self-adjusting air inlet made of programmable carbon fiber, which would replace the heavy mechanical system which is currently being used[7]. Apart from aerospace, a number of industries are expected to take advantage of 4D printing including automotive, construction, healthcare, clothing, defense and military.

A growth of around 162 million USD by 2022 is expected to be seen in the 4D printing market and a compound annual growth rate (CAGR) of nearly 39% between 2019 and 2022[8]. While programmable carbon fiber might hold the largest market share, programmable wood grain and programmable fabrics are expected to grow at an appreciable rate by 2025[9]. The overall 4D printing market is expected to be a $537.8 million industry by the end of 2025[10].
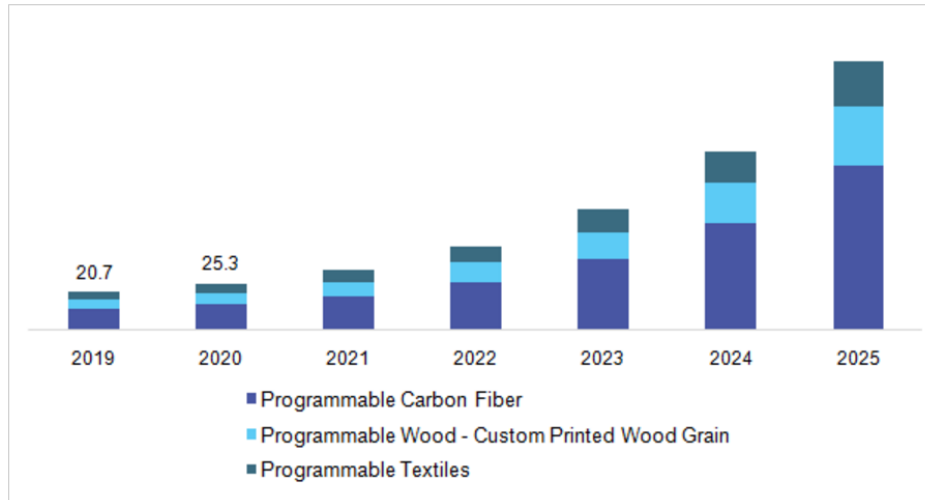
Figure 2-6 U.S. 4D printing market by material, 2019 - 2025 (USD Million)[11]

Most of the current 4D printing systems depend on polymer systems to achieve shape change as polymers are more versatile and it is easier to manipulate their properties as compared to shape memory alloys or any other system. The early 4D printing systems consisted of multiple polymers such that internal stresses in one layer or one part of the 3D printed object led to a shape change in the object. The more recent 4D printing systems have been focusing on the use of single material systems which facilitate the ability to fabricate complex shapes, unlike multi-material systems which depend on hinges and connectors which cannot be embedded into complex shapes.

2.2.2 Multiple material based 4D printing

For multi-material 4D printing systems, internal stresses in specific parts of the object have to be programmed accurately to obtain a shape change. These sites of stresses can be generated either by using hydrogels or by using Shape Memory Polymers (SMPs).

When using hydrogels, swelling of the hydrogel at particular sites is controlled by an additive which can influences the extent of swelling. A system of this kind included inks made up of a thermoresponsive polymer poly(N-propylacrylamide) (NIPAM) and poly(2-

10

hydroxyethyl methacrylate) (HEMA) whose swelling was modified by the use of a polyether-based polyurethane[12]. Both the inks were extruded are different rates and a UV lamp was used to polymerize the deposited inks. This allowed to print an object with hinges which could be controlled to swell disproportionally causing them to bend to a desired shape.
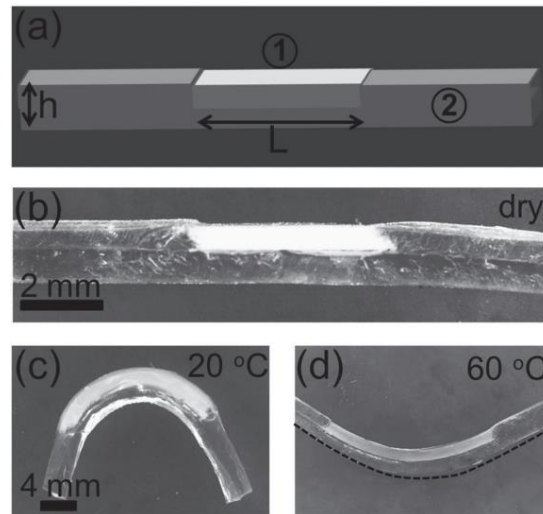
Figure 2-7 (a) Model of a thermosensitive hinge with (1) made of PNIPAm and (2) made of poly(HEMA); (b) dry, as-printed sample; (c) hydrogel swollen at 20°C; (d) deswelled hydrogel at 60°C

Another way is to use Shape Memory Polymers (SMPs) to print objects having layers of two different polymers, one of which is the SMP that responds to temperature change and the other an elastomer layer which has an internal biaxial compressive strain which can be programmed using the curing time and intensity[13]. These two layers bond to each other to form a flat laminate and the compressive strain gets coupled by the SMP layer as the modulus of the SMP layer is higher than the elastomer layer at room temperature. When the temperature of this system increases above the glass transition temperature of the SMP, the compressive strain inside the elastomer layer gets released as the modulus of the SMP decreases and the laminate bends to acquire a shape. This simple technique can

be modified by strategically placing the elastomer and SMP layers to print complex shapes like a helix, a dome or even a buckyball.

(a)

(b)
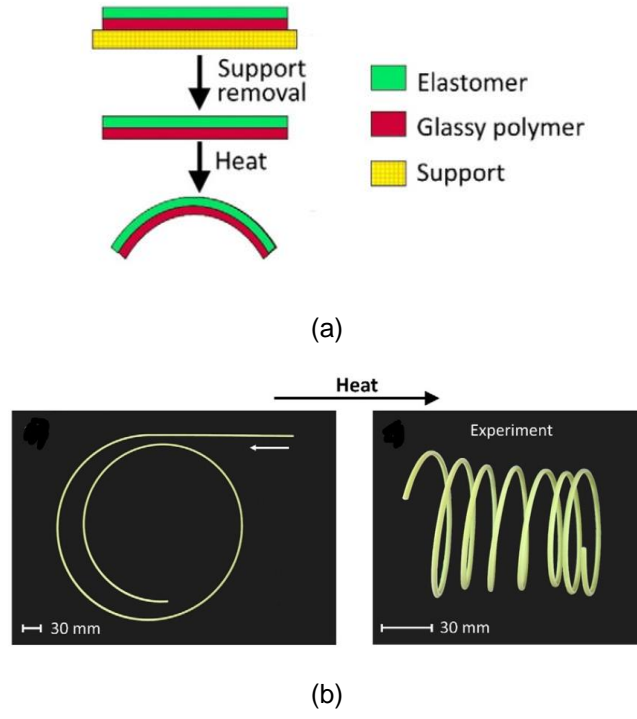
Figure 2-8 (a) Elastomer bonded to glassy polymer forming a flat laminate whose shape changes by application of heat; (b) Helix being formed by application of heat

2.2.3 Single material based 4D printing

With the multi-material method, only relatively simple geometric shapes can be printed. Complex shapes containing smooth curves require extremely precise placement of material which could lead to an increase in fabrication time. To counter this, single material systems which consist of a single homogenous phase are used for printing which can then be actuated by appropriated stimuli mechanism.

An ink containing poly(lactic acid), dichloromethane, and benzophenone was used a process similar to FDM printing along with UV LEDs shining on the deposited ink to

immediately cross-link the poly(lactic acid) chains for a shape memory behavior. To provide an actuation mechanism, Fe_3O_4 particles were embedded into the ink so that heating could be induced remotely by alternating magnetic field. A spiral scaffold was programmed to show a self-expansion behavior to demonstrate the system[14]. Another system used a hydrogel ink containing stiff cellulose fibrils which underwent alignment due to shear. This gave rise to an anisotropic swelling behavior when immersed in water and could induce complex shapes due to uneven swelling in the printed structure[15].

(a)   (b)
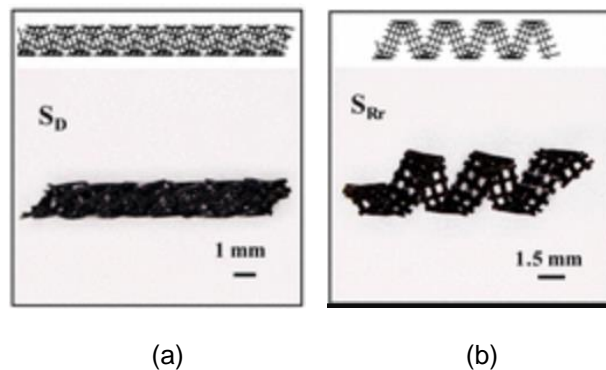
Figure 2-9 (a) deformed state; (b) recovered state

In a more recent approach, an ink composed of hydrophilic poly(hydroxyethyl methacrylate) was exposed with light of varying intensity which allowed for variable cross-linking density to fabricate a flat sheet which when immersed in water changes shape as programmed by the light intensity and crosslink density[16].

2.3 Nanocomposites

3D printing has been used to demonstrate the ability to print complex ceramic as well as metal objects using 3D printing techniques including FDM and SLA. To be classified as a nanocomposite, at least one of the composite material should be in the nanometer scale. The can be nanopowders, nanorods or any kind of nanoparticles. These fillers mainly act as reinforcing agents to which enhanced mechanical properties can be attributed. Special fillers can be used which impart other properties to the composite. Magnetic nanoparticles

provide magnetic properties while some of the fillers provide conductive properties. A considerable amount of research has been done in the field of 3D printed nanocomposites.

60% by weight Copper powder was dispersed in a system containing a monomer, a photo-initiator and a dispersant and was 3D printed using the stereolithography process to obtain a green body. This was then subjected to a temperature profile with dwell step at 600°C for polymer burnout and another dwell step at 950°C for sintering of the copper particles. A pure copper object was obtained at the end of this temperature treatment and a shrinkage of 22-28% was observed due to polymer burnout. The object was tested for electrical conductivity and was it was found to match other metals[17].
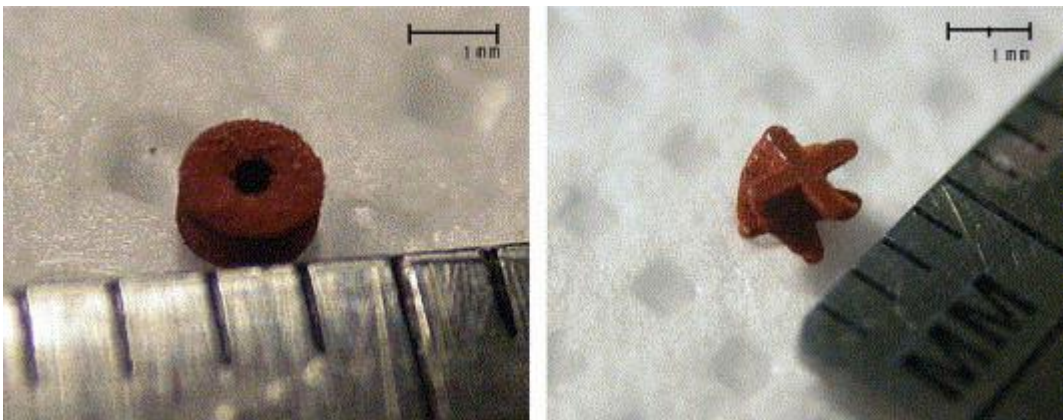
Figure 2-10 Samples with copper and polymer binder

A similar system was demonstrated with a different polymer ink system containing metal powder of Cobalt and in a system with same polymer ink system along Tungsten Carbide powder, both at 60% by weight[18].

In recent research, 3D printing was used to fabricate nanocomposites using silica nanoparticles. When processed further and sintered, a consolidated transparent glass object was obtained. In the first paper, hydrophilic fumed silica nanoparticles (23% by wt) were suspended in tetraglyme (tetraethylene glycol dimethyl ether) with

poly(dimethylsiloxane) to obtain an ink for Direct Ink Writing (DIW). The printed green body was subjected to drying at 100°C for 110 hours followed by heating at 600°C for 2 hours to burnout the organic components of the nanocomposite[19]. Only simple printed structures without complex curvatures were shown in the paper.
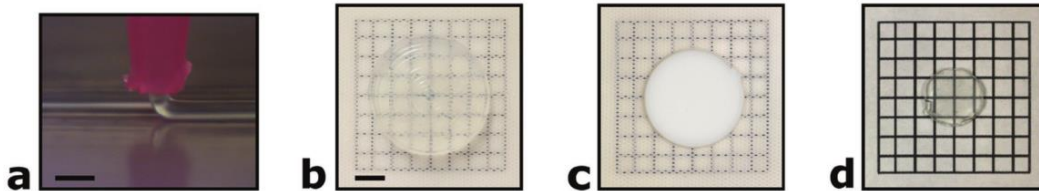
Figure 2-11 (a) DIW of silica filled ink; (b) printed part; (c) dried part consisting of bound silica powder; (d) densified glass part

Another group used a precursor made of silica nanoparticles (37.5 % by wt) dispersed in a monomeric matrix of hydroxyethylmethacrylate, tetraethylenglycoldiacrylate and phenoxyethanol for stereolithography. The polymer burnout was performed at 800°C for about an hour. The green body was further sintered at a temperature of 1300°C at a pressure of 5×10^{-2} mbar[20].
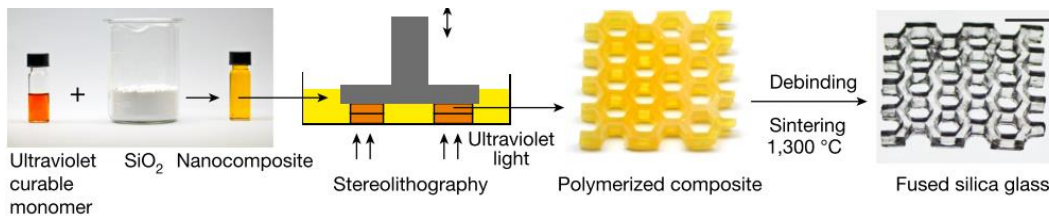
Figure 2-12 Process for fabricating fused silica glass component by stereolithography

2.4 Sheet forming

Sheet metal forming is one of the popular metal shaping technique used in numerous industries worldwide due to its ease of operation and capability for mass production. Large quantities of thin sheet metal can be manufactured by modern rolling mills which is then formed using secondary processes for industries which deal in automobiles, aircrafts, food

and beverage cans and other industries. Some of the common forming process are blanking, bending, stretching, hole extrusion, stamping among many others[21]. Most of these processes are cold working processes meaning that the metal sheet is not heated prior to deforming it. Dies are used to shape the sheet based on the type of forming required. One of the advantage is that one metal sheet can be operated on by multiple dies which can be done in a single step at the same time which makes it a very time efficient process. A major disadvantage is that a mold or die is required for each new shape requirement and the manufacturing of a new mold is expensive, as it has to be made reliable for a large number of repeated operations.
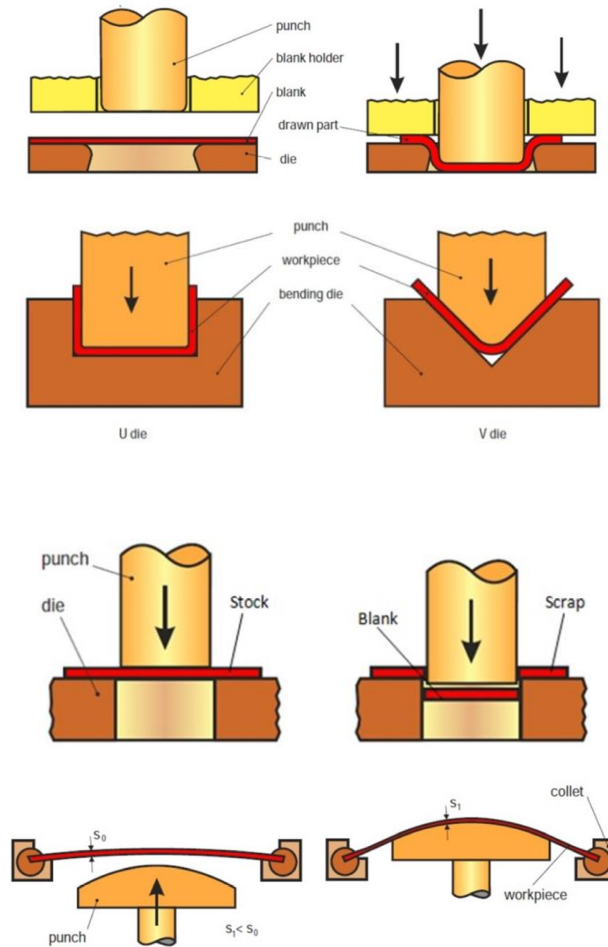
Figure 2-13 Drawing, Bending, Blanking, Stretch Forming[22]
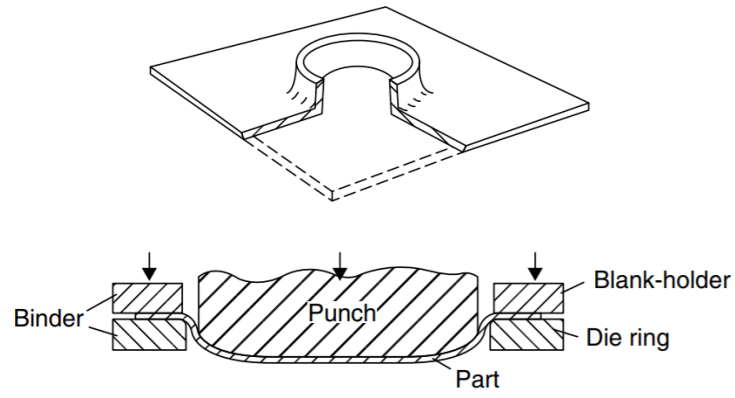
Figure 2-14 Hole extrusion and stamping

Chapter 3

Background

3.1 Mechanical instabilities in flat plates

3.1.1 With external constraints

Consider a flat body at equilibrium with length L and thickness t. If the body is compressed

by δ from both sides, then a total of 2δ compression is obtained.
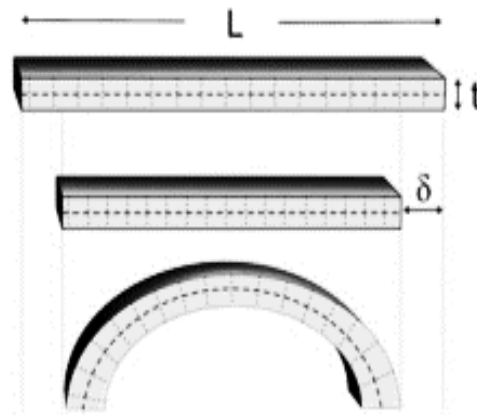
Figure 3-1 Compressing a body by 2δ

Now, it can be shown that the energy per unit area in this compressed body can be written

as $E_s = C(\frac{\delta}{L})^2 * t$. If we consider the body to obey up-down symmetry, we observe a flat

configuration termed as pure stretching deformation. If the system were to break the up-

down symmetry, the body would bend either upwards or downwards. Here, if the radius of

curvature is appreciably larger than the thickness of the body, the material lines normal to

the mid-plane remain normal even after bending.

It can be shown that the bending energy is $E_B = C'K^2t^3$ and is known as the pure bending

configuration. If the thickness is decreased, the stretching energy decreases linearly which

the bending energy decreases non-linearly at by the order of three. Below a certain thickness, the bending energy is lower than stretching energy and hence bending is more favorable than stretching. This is when the body prefers to bend in order to relieve the internal stress.

3.1.2 Without external constraints

Shaping of flat bodies without external confinements can be another scenario which can be studied. In these bodies, non-uniform growth can lead to development of internal stresses and cause buckling instabilities even when there is no constraint present for the body.

Figure 3-2 Non-uniform in-plane growth

19

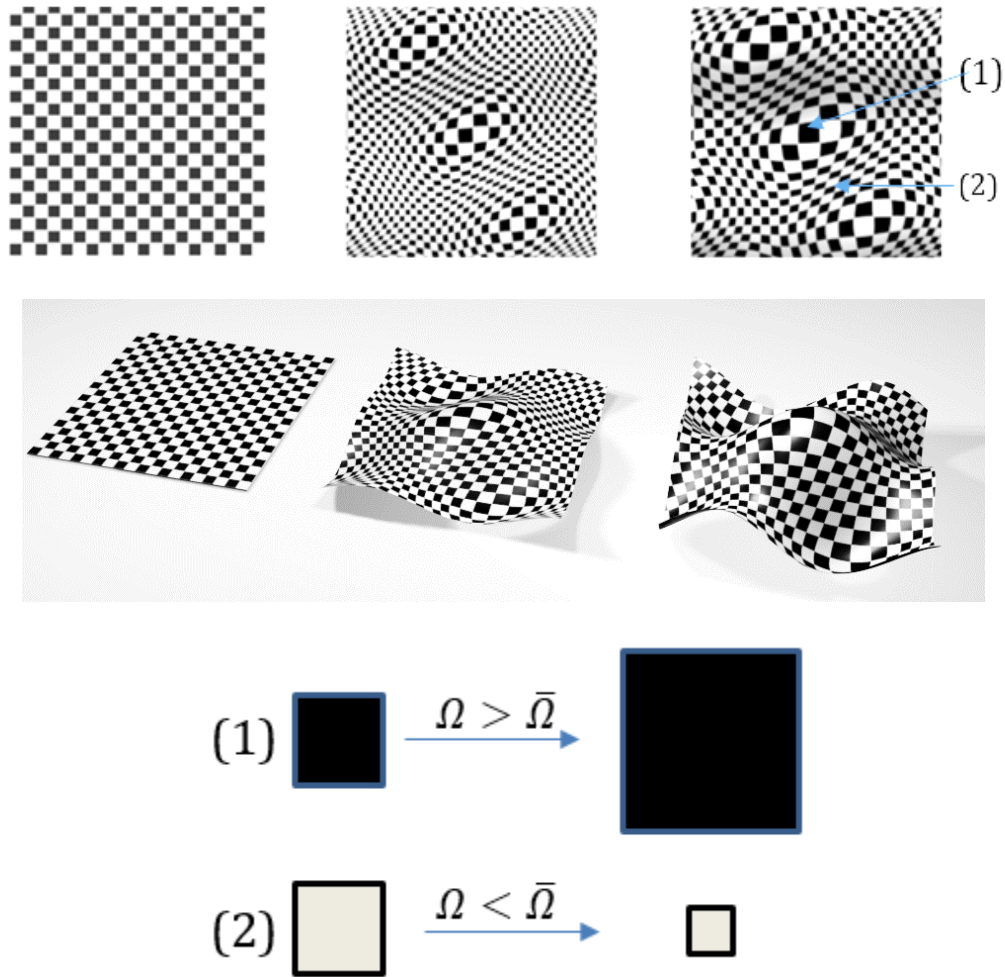It is important to remember that one-dimensional growth simply leads to non-uniform growth while for two-dimensional bodies, a majority of the portion of the residual stress can be relieved through energetically inexpensive bending.

3.2 Non-Euclidean plates

Non-Euclidean plates are stacks of identical surfaces having 2D intrinsic geometry which is not Euclidean and hence cannot be realized in a flat configuration. In nature, we find several non-confined 2D structures which undergo non-uniform in-plane local growth which develops internal residual stresses and lead to an out of plane deformation such as buckling or wrinkling. This can be seen in natural bodies with soft tissue like plant tissue or skin.

A metric is defined as a non-negative function which describes the distance between neighboring points for a given set. The shape of a surface, i.e. its configuration in space is described by the metric in space. But the metric alone does not specify the configuration, to select a specific shape the local curvatures on the surface are also needed to be determined.

To understand the non-Euclidean surfaces talked about in further experiments, we need to understand Gaussian Curvature. The curvature of a plane curve as a point is the reciprocal of the radius of a unique circle which most closely approximates the curve at the point. Knowing this, we understand that the curvature of a circle is the same everywhere on its perimeter or that the curvature of straight line is zero. If we choose a point on a surface, a normal vector can be drawn and there can be numerous planes which contain this normal vector and intersect the shape to give curves which are termed as normal curves. To better define the curvature at this point, called the Gaussian curvature, we consider two normal curves which give the maximum and minimum values and are termed as the principal curvatures k_1 and k_2. The Gaussian curvature, K, is the product of these principal

20

curvatures, i.e. $K = k_1 \cdot k_2$. Knowing this, we can now classify surfaces based on their Gaussian curvatures. If one of the principal curvatures is zero, the Gauss curvature is also zero and this surface is known as a developable surface meaning that it can be developed from a plane without tearing or stretching and also flattened into a plane.
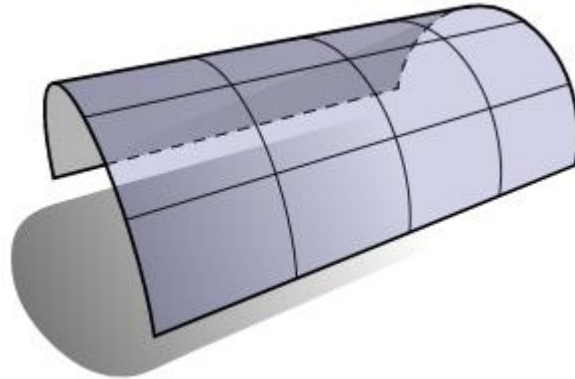
Figure 3-3 Surface with zero Gaussian curvature

If both the principal curvatures have same signs, then the Gaussian curvature is positive as the product of the principal curvatures is greater than zero. Here, the entire surface lies on one side of the tangential plane to the point at which curvature is being measured. An example of a surface with positive curvature is a hemisphere.
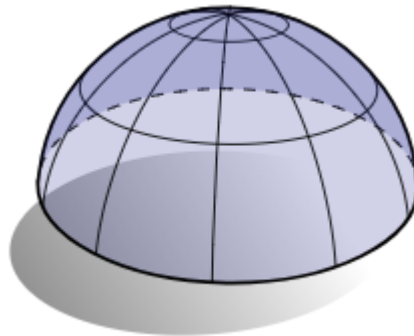
Figure 3-4 Surface with positive Gaussian curvature[23]

Next, if the principal curvatures have different signs, the Gaussian curvature turns out to be negative. This gives a hyperbolic surface or a saddle like surface.

21
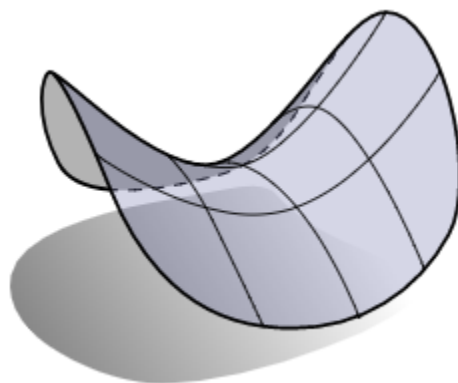
Figure 3-5 Surface with negative Gaussian curvature

3.3 Poly (N-isopropylacrylamide)

Smart polymers are polymers, which can respond to external stimuli by a change in their structure or properties. External stimuli like pH, temperature, magnetic field, etc are commonly used to activate changes which are reversible, meaning that after removal of the stimuli, the system goes back to its initial state. Polymers which respond to temperature are termed as thermosensitive and Poly (N-isopropylacrylamide) (PNIPAm) is one such polymer. Since its first synthesis in the 1950s, PNIPAm has been the most studied thermosensitive polymer due to its unique thermal behavior in aqueous media. It possesses the property of inverse solubility upon heating above a certain temperature, which is quite contrary to the behavior of other polymers in organic solvents. This sharp transition from a state of hydrophilicity to hydrophobicity is known as the lower critical solution temperature (LCST) which is a major part of research, especially in the biomedical field for controlled drug release. The LCST can vary between 32 and 33°C but is independent of molecular weight and concentration[24].

Figure 3-6 PNIPAm repeating structure

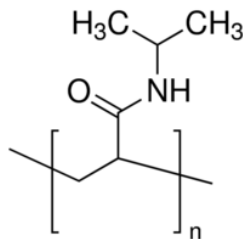The NIPAm monomer is an organic amide with isopropyl and acryloyl in the side chain. The acryloyl group contains a double bond which serves to provide a functionality of two when the monomer is polymerized by free radical polymerization. When polymerized, a linear chain is obtained. To obtain a gel, crosslinks are required to be present between these chains and this is achievable by having additional monomers with functionality of two present while NIPAm is being polymerized by free radical polymerization. One such widely used crosslinking monomer is N,N′-Methylenebis(acrylamide) because of its structural similarity with NIPAm.
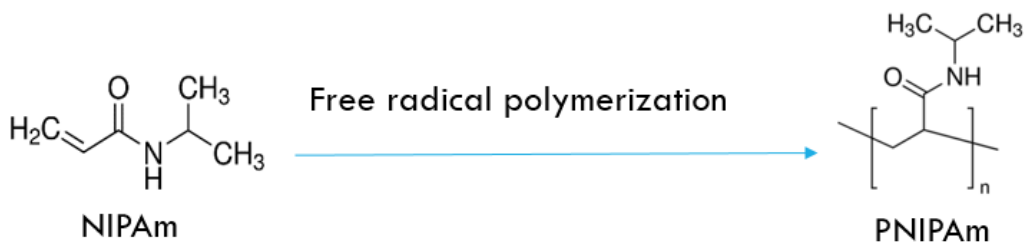
Figure 3-7 Free radical polymerization of NIPAm
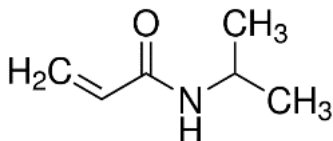
Figure 3-8 Structure of NIPAm

NIPAm hydrogels were used in making non-Euclidean plates as the samples undergo differential swelling and deswelling due the collapse of the polymer chains leading to second phase with lower polarity. One of the theory of LCST states that below the transition temperature, PNIPAm chains order their amide groups to form hydrogen bonds with the already arranged water molecules, which then gives a negative enthalpy term and dominates the Gibbs free energy. The entropy decreases because of the water molecules reorienting around nonpolar regions of PNIPAm.

$$\Delta G = \Delta H - T\Delta S$$

The negative Gibbs free energy leads to water absorption. As the temperature increases above the transition temperature, the entropy term becomes dominant which causes water release and results in phase separation.

3.4 Previous experiments on fabrication of non-Euclidean plates

An example of a non-Euclidean plate is when a thin disc of radius R and thickness t undergoes uniform isotropic growth for a radius r which is smaller than R. If we consider the disc to have a flat configuration without any bending due to the growth, compressive stress develops in the inner part of the disc while the outer part is under tension. If a flat configuration is not considered, bending is seen due to buckling out of plane in the form of a 3D configuration.[25] To demonstrate this experimentally, thermoresponsive, N-isopropylacrylamide (NIPA) gel was made which showed a sharp volume reduction at 33°C due to the LCST of the monomer. Multiple gel discs were prepared with varying monomer concentration and the shrinking ratio was measured by immersing the discs in water at a temperature of 45°C, which showed a strong dependence of the monomer percentage present on shrinking ratio. The shrinking ratio or normalized length was obtained as the diameter of warm gel disc divided by the diameter of the original diameter of the disc. Concentrated gels shrink less while dilute gels shrink to a larger extent.
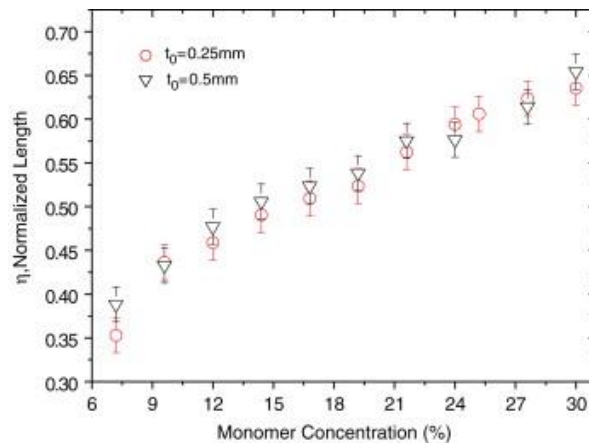
Figure 3-9 Calibration of NIPA gels[26]

24

This served as the calibration for further experiments in which discs were generated by polymerization of a combination of high and low concentrations of NIPA solutions. The discs thus obtained had radial gradients of concentrations such that when immersed in water having temperature greater than the LCST, differential shrinkage occurs along the radius of the disc, which forms a non-Euclidean shape.
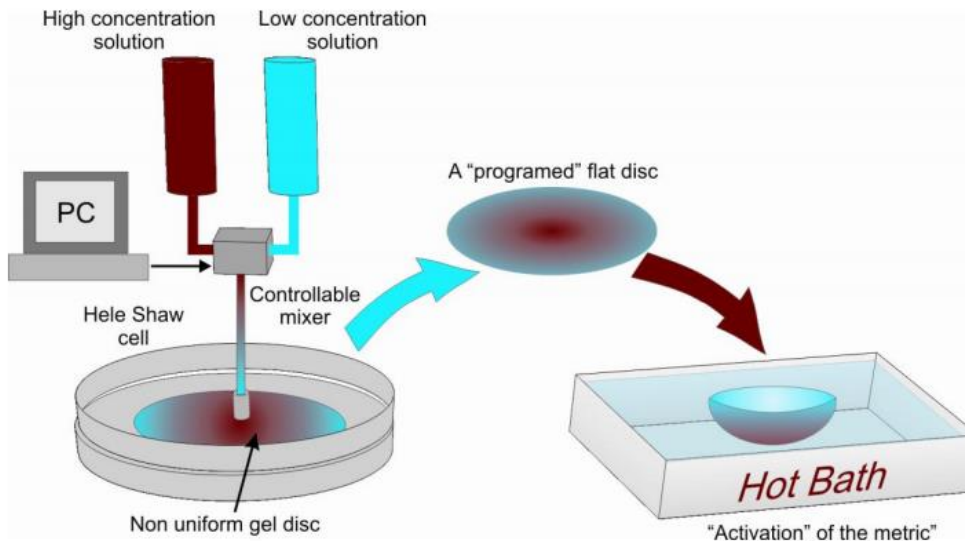
Figure 3-10 Generation of discs with varying monomer concentration

These discs can be programmed with a variety of gradients which are responsible for specific shape changes when immersed in warm water[27].

Figure 3-11 Programmed 3D shapes

This method is useful only for symmetrical shapes varying radially which is a major drawback. This drawback was addressed by using a technique called Halftone Gel Lithography which was based on the same principle used in the previous study except that they used lithography to program the discs. The swelling ratio here is defined as the area of homogenous film in a fully swelled state divided by the area in the dry state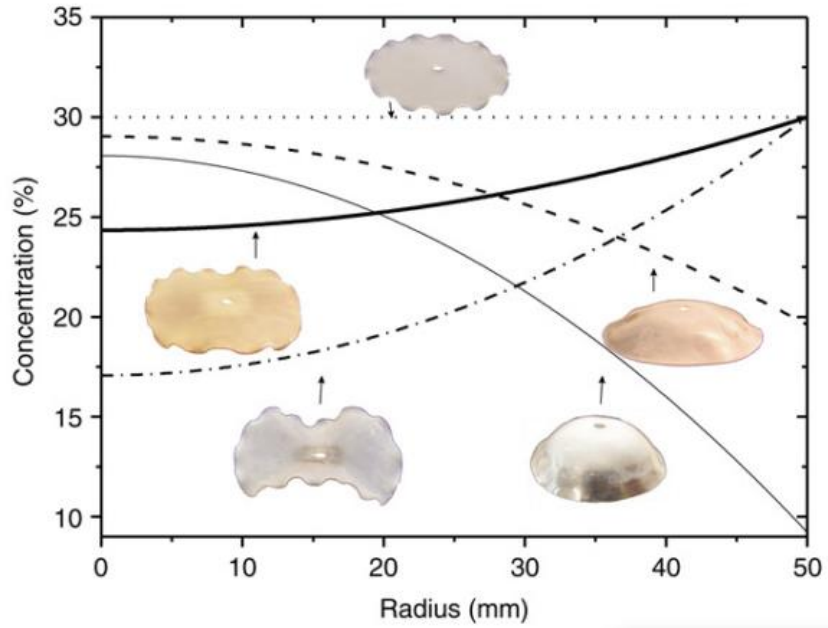. The maximum and minimum swelling ratio was determined by illuminating the copolymer film with varying dose of UV light through the first photomask. The smallest amount of dose required to gel the film also allows the gel to swell the most in water. After this, a second photomask is used to provide a high dose of UV to pattern circular dots of diameter d which have the lowest amount of swelling in water. This difference in swelling due to high crosslink density in areas with high UV dose while the low UV dose region has lower crosslink density. The lattice spacing of the dots is constant while the diameter can be manipulated as required. The system is calibrated by changing the fraction of the dots by manipulating their diameter. It was observed that with an increase in the fraction of dot percentage led to the lowering of the overall areal expansion ratio and converges at a temperature around 45^OC. This data was then used to fabricate halftone discs with

axisymmetric programmed shapes by changing the dot diameters over the surface of the disc including those of a saddle and a dome. This method relies on the elasticity of the gel to smooth out the contrast in swelling between areas of high and low crosslinked areas to provide an intermediate swelling.
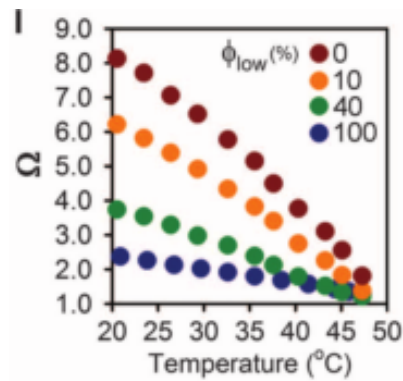

Figure 3-12 Temperature dependence of swelling ratio on the fraction of dots

Knowing the swelling factors, the target curvature at a point r of the material is written in terms of the coordinates on the swelled gel sheet.
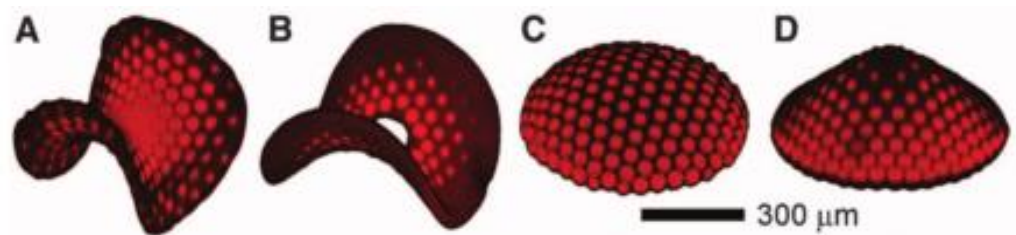

Figure 3-13 (A) Saddle Surface (Sa); (B) Cone with excess angle (Ce); (C) Spherical cap (Se); (D) Cone with a deficit angle (Cd)
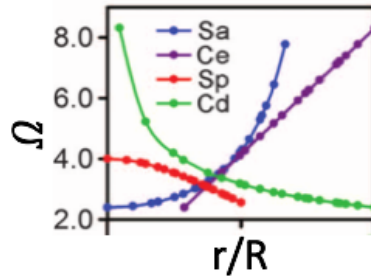
Figure 3-14 Swelling factors as a function of normalized radial position

The above is an effective technique but the use of continuous and larger number of masks would allow for better gradations in the swelling of the discs. This type of mask generation is possible in 3D printers which use DLP projection system to print layers made by crosslinking the polymer which would effectively act as non-Euclidean plates if the printed objects are swelled in water. For this to be possible, NIPAm monomer will be used in this study to print a flat programmed shape. We calibrate the system with silica nanoparticle precursor to determine the highest and lowest possible amount of crosslinks and hence the swelling ratio. This data is then used to generate appropriate masks required to obtain shapes with negative, positive and zero Gaussian curvature surfaces and then dry them such that they are able to retain their shape in air. We perform these experiments to demonstrate the effectiveness of our technique to fabricate nanocomposites using 4D printing based on the previous studies.

Chapter 4

Experimental

4.1 Objectives

1) Study the effect of nanoparticle loading on shape forming behavior and compare with pure polymeric precursor

2) To fabricate principle shapes and determine the printing accuracy

3) To establish a process to stabilize the deswelled shapes in air

4) To evaluate physical, mechanical and system dependent properties of the solid shapes

4.2 Theory

On a 2D sheet, we prescribe the target metric $\bar{g}$, such that it results in a non-zero Gaussian surface (non-Euclidean metric), the resulting configuration of the sheet would be completely free of in plane strain (stretching energy). Such a free sheet will acquire a 3D configuration to minimize its elastic energy. For a sheet of vanishing thickness, an isometric embedding of the target metric having the lowest bending energy is adopted. If the stress free flat disc has a metric of g, and whenever $g \neq \bar{g}$, there are a few "springs" (two points which are strained) which are not at their rest lengths and results in a local strain. This local strain at each point is the discrepancy between the metric of the given configuration and the target configuration.

$$\varepsilon = \frac{1}{2}(g - \bar{g})$$

The equilibrium distances between points are thus determined by planar growth to attain the target metric $\bar{g}$.

We consider a surface which is parametrized by two parameters (η^1, η^2) which are collectively shown as η. r is the position vector of points on this surface and ds is the line element on the surface which satisfies

$$ds = h_{ij}d\eta^i d\eta^j \qquad (1)$$

where,

$$h_{ij}(\eta) = \frac{\partial r}{\partial \eta^i}\frac{\partial r}{\partial \eta^j} \qquad (2)$$

Suppose now a piece of paper is used to obtain this surface in a way such that distance between points near each other at the plane is deformed, and if (ξ^1, ξ^2) (collectively ξ) are the Cartesian coordinates on the plane before deformation, the line element that satisfies after deformation is

$$ds^2 = g_{ij}d\xi^i d\xi^j \qquad (3)$$

here, g is the deformed metric whose elements depend on ξ. Before deformation of the plane, dl would have been the line element,

$$dl^2 = \delta_{ij}d\xi^i d\xi^j \qquad (4)$$

For a conformal deformation, we can write,

$$g_{ij} = F^2\delta_{ij} \qquad (5)$$

where F is a scalar called scale function depending on ξ and $F^2 = \Omega$ which is defined as the areal growth function. Equating (1) and (3), and using (5) we have,

$$h_{ij}(\eta) = F^2(\xi)\delta_{kl}\frac{\partial \xi^k}{\partial \eta^i}\frac{\partial \xi^l}{\partial \eta^j} \qquad (6)$$

We thus get three independent equations which can be used to find the three unknowns ξ^1, ξ^2 and F if components of h are known functions of η. Or, if F is a known function of ξ with any choice of η in terms of ξ, the components of h can be found from (6) which can then be used to find the r from (2).

According to Gauss's Theorema Egregium, Gaussian curvature is then,

$$K = \frac{-\Delta(ln\lambda)}{\lambda^2} = \frac{-\Delta(ln\Omega)}{2\Omega} \qquad (7)$$

where Δ is the Laplacian operator. We can thus obtain the areal growth function and determine the 3D shape.

Theoretical model of axisymmetric 3D shapes:

In a cylindrical coordinate system (ρ, φ, z), where z-axis is the axis of symmetry (axis of rotation) and $z = f(\rho)$, we consider an axisymmetric 3D shape (surface of revolution). Then, the square of the element of arc length in the surface, ds²,

$$(1 + f_\rho^2)d\rho^2 + \rho^2 d\varphi^2 = \Omega(r)(dr^2 + r^2 d\theta^2) \tag{8}$$

where, $f_\rho = \frac{df}{d\rho}$. The right-hand side of equation (7) describes how the growth function Ω changes the distance dl between points on undeformed 2D plane (polar coordinate system) to the distance ds on the 3D surface (cylindrical coordinate system). As we know the deformation is axisymmetric, we assume that the angle between the two points in 2D and 3D do not change and hence, $d\varphi = d\theta$ and $\rho^2 d\varphi^2 = \Omega(r)r^2 d\theta^2$. Then from (8), we get,

$$\rho^2 = \Omega(r)r^2 \tag{9}$$

$$(1 + f_\rho^2)d\rho^2 = \Omega(r)dr^2 \tag{10}$$

Thus, we can find the between r and ρ, and Ω and ρ. The 3D shape can be determined for given Ω using (9) and (10).

Determination of growth function for 3D shape:

We determine the target metric, i.e., the growth function, Ω for a spherical cap from its 3D shape. A spherical cap of radius r_o is given as,

$$\rho^2 - (z - z_o)^2 = r_o^2 \tag{11}$$

Where, z_o is a constant. Using (9), (10) and (11),

$$\rho = \frac{2r_o(r/R)}{1 + (r/R)^2} \tag{12}$$

$$\Omega = \frac{c}{(1 + (r/R)^2)^2} \tag{13}$$

31

Where $c = 4(r_o/R)^2$. We can get the local Gaussian curvature $K = \frac{1}{r_o{}^2} = \frac{4}{(cR)^2}$ using (7) and

(13).

Now we determine Ω for a cone shape from its 3D structure. The equation of a cone with

vertex angle of 2ß is given by,

$$z - z_o = \rho \cot \beta \qquad (14)$$

We obtain ρ and Ω as a function of r using (9), (10) and (14),

$$\rho = \rho_o (\frac{r}{R})^\alpha \qquad (15)$$

where, R is a constant and α = sinβ, and

$$\Omega = c(\frac{r}{R})^{2(\alpha-1)} \qquad (16)$$

where, $c = (r_o/R)^2$. We obtain K=0 using equations (7) and (16)

For a saddle shape, we use

$$\Omega = \frac{c}{(1-(r/R)^2)^2} \qquad (17)$$

From this, we obtain $K = \frac{4}{(cR)^2}$ using (7) and (17)

4.3 Dynamic Mask Photolithography

DLP technology can be used to fabricate cross-linkable networks using its ability to fabricate complex patterns. DLP allows micro-tuning of the photo-exposure (known as gray-scale lithography) without the need of rigorous mask alignment as required for common multi-step photo-lithography. The response of the precursor system has to be photo-tunable during photo-polymerization. The dynamic mask generator used was a commercial video projector (Vivitek D912HD) with a filtered Mercury-vapor lamp working at 70 Watts (3500 Lumens with a lamp efficiency of 50 lm/Watts). Each set of masks are generated based on the theory for a particular shape.
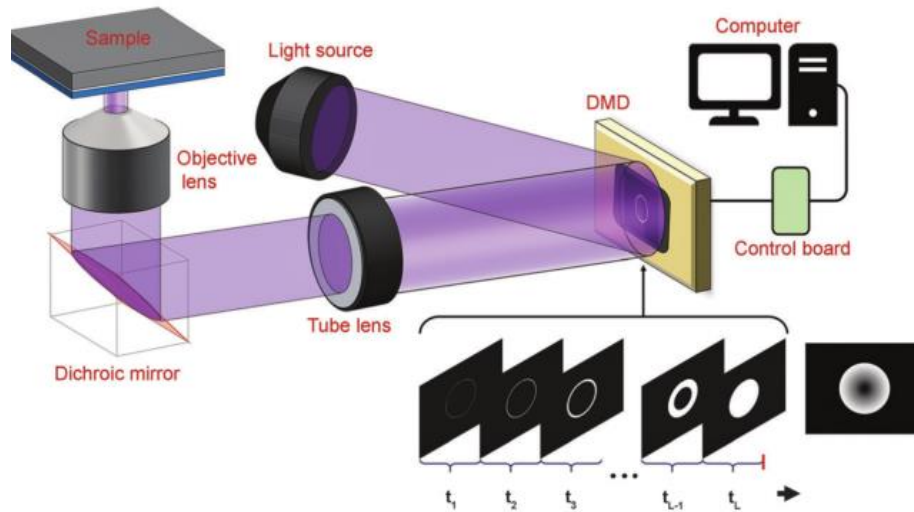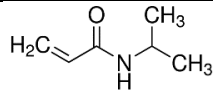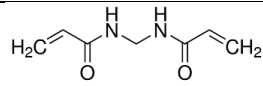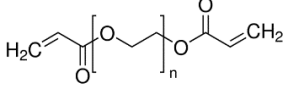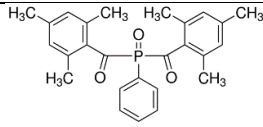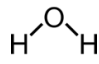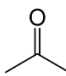
Figure 4-1 DLP projection system

4.4 Experimental

4.4.1 Materials

Aerosil OX50 amorphous silica nanopowder having average particle size of 40nm was provided by Evonik Industries. N-Isopropylacrylamide [NIPAM] stabilized with MEHQ was purchased from TCI America. N,N′-Methylenebis(acrylamide) [MBAM], Poly(ethylene glycol) diacrylate [PEGDA] and Phenylbis(2,4,6-trimethylbenzoyl)phosphine oxide were purchased from Sigma-Aldrich. All the materials were used as obtained.

Table 4-1 Materials

Component	Function	Structure
N-Isopropylacrylamide	Monomer	
N,N′-Methylenebis(acrylamide)	Crosslinker	
Poly(ethylene glycol)diacrylate	Crosslinker	
Phenylbis(2,4,6-trimethylbenzoyl)phosphine oxide	Photo Initiator	
DI Water	Diluent	
Acetone	Diluent	

4.4.2 Precursor and Ink preparation

A 10% by weight aqueous master solution of PEGDA was prepared. A photoinitiator master solution was made in a proportion of 1:39.5 from Phenylbis(2,4,6-trimethylbenzoyl)phosphine oxide and acetone respectively. The precursor was made using 0.4 g NIPAM, 32 µL PEGDA master solution, 5.44 mg MBAM in 0.09 g photoinitiator master solution, 222 µL De-Ionized Water and 630 µL acetone.

Composite precursors were made of Silica nanoparticles with 5%, 10%, 20% by weight solid loading.

4.4.3 Fabrication of the nanocomposites

The reaction cells were made of a PDMS substrate and a glass slide separated by PDMS spacer having a height of 400±0.5 μm. Prior to printing, the composite precursors were bubbled with nitrogen for a minute to avoid oxygen interference. A commercial projector having 1920x1080 pixels with a 30μm resolution was used for Greyscale gel lithography to cure the samples with 25 exposures of 2 second each. These samples were detached from the glass slide and washed with isopropyl alcohol to suppress further polymerization. The samples were stored in DI water at 4°C for a day to eliminate any unreacted monomer present.
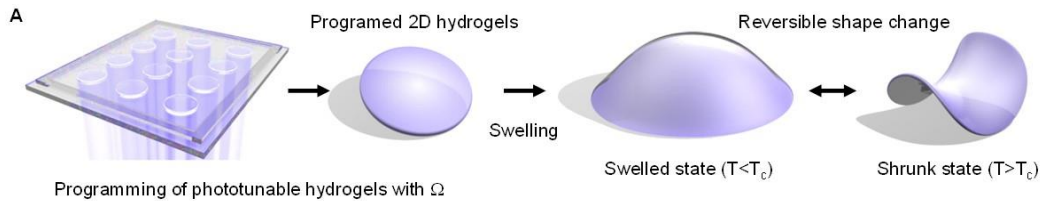

Figure 4-2 Fabrication cell

4.4.4 Calibration

Owing the 3D transformation of 2D printed samples to areal swelling and deswelling in water due to temperature change, the effect of exposure time and composition of the precursor is an important factor for determining exposure patterns required for complex 3D transformations. The swelling ratio was defined as the area of swelled sample by are of the swelled sample by the area of the printed samples. The deswelling ratio (Ω) was defined as the area of the deswelled samples to the area of the printed samples. To measure these ratios, samples having diameter of 7mm were printed with digital masks for different exposure times. The areas of the individual samples were measured just after washing with isopropyl alcohol. The samples were allowed to swell in water at 4°C for a day and the area measured, after which the gels were subjected to slow heating over the

35

LCST of 33°C at which point they were kept in the heated water for 12 hours to ensure that most of the water was expelled from within the gel due to the LCST transition.

4.4.5 Drying

Temperature of the water bath was increased from 33°C to 50°C to increase the NIPAm water repulsion. After an hour, the medium of the samples was changed to a near saturated NaCl salt solution (20% by wt) to induce a volume phase transition while keeping the temperature constant at 50°C. After 30 minutes in the ionic environment, the samples were placed on an absorbent tissue to eliminate as much water as possible and left to dry in the oven.

4.4.6 General scheme for solid fabrication

In previously mentioned researches, PNIPAm hydrogels were fabricated using Hele-Shaw cells and halftone lithography, but to achieve a smoother gradient multiple exposures of suitable digital patterns are required. We use a commercial projector to expose the precursor to these digital patterns which perform selective crosslinking. The grayscale patterns are generated by conformal mapping of the desired target shape taking in consideration the growth pattern of the hydrogel which is required for the shape to be realized and the physically achievable growth range of the material. The grayscale exposure of the patterns takes less than 60 seconds to complete. The exposed precursor area undergoes crosslinking and forms the printed shape which is detached from the glass slide, washed and the swelling and deswelling by temperature change is done to obtain the target shape. This is followed by the drying step which gives the final dry shape.
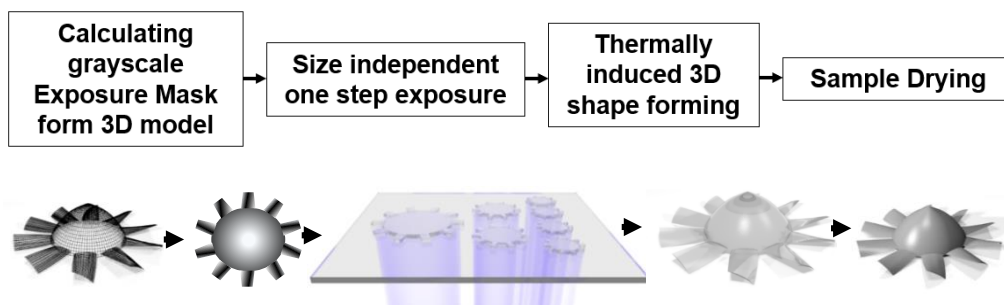
Figure 4-3 Overall scheme for printing flat hydrogel sheets

The advantage of this method of printing is that a single exposure step is required for any size of initial lateral print required for the final shape. This is possible because of the 2D to 3D transformation by swelling which does not depend on layer by layer printing as in conventional 3D printing techniques.

4.5 Results

4.5.1 Calibration

To understand the areal growth due to swelling and deswelling behavior of the gels as a function of the pattern exposure time, we perform calibration for each precursor. We expect to find low shrinkage in precursors with high solid loading. This is due to the fact that the presence of higher amount of solids are expected to not allow deswelling to the same extent as in precursors with no solid loading. This was experimentally confirmed as shown in the figure.
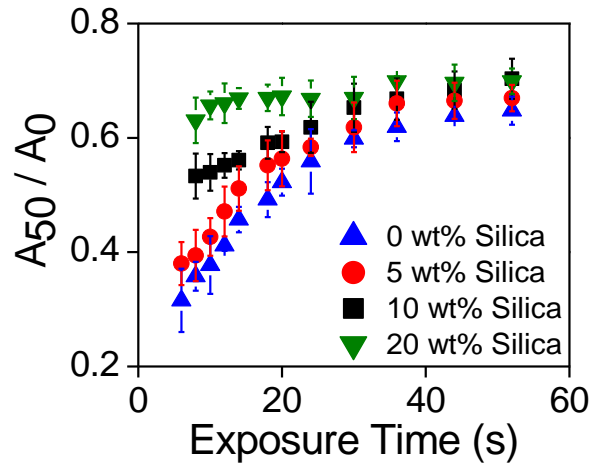
Figure 4-4 Calibration curves for precursors

As seen above, the deswelling ratio increases with increasing solid loading for the lowest exposure time. This correctly indicates that deswelling is difficult for samples with higher solid loading. The difference between minimum and maximum deswelling ratio should be as high as possible to be able to fabricate accurate shapes. As this working range decreases, the capability of diverse shapes to be printed from the particular precursor also decreases. The 5% solid loading samples have a calibration range (~0.39 to 0.64) which is comparable to the pure precursor (~0.32 to 0.62).

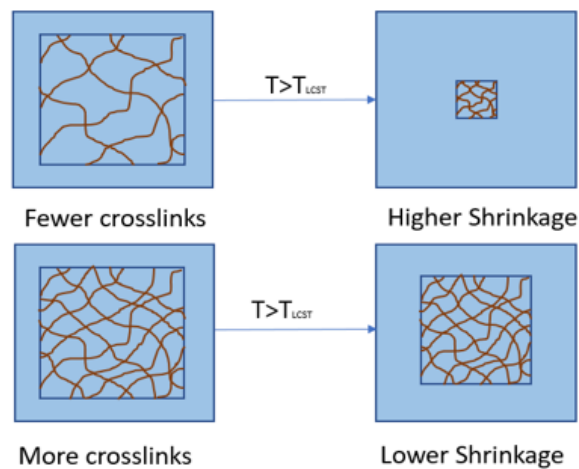

Figure 4-5 Shrinkage dependent on crosslink density

4.5.2 Fabrication of principle shapes and accuracy

Using this above calibration data, we show principle shapes having positive and negative

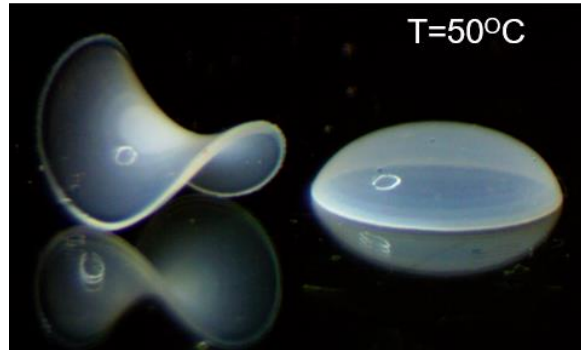curvatures at a temperature of 33°C in water. Cones with deficit angles were also printed.

Figure 4-6 5% silica principle shapes at 50°C
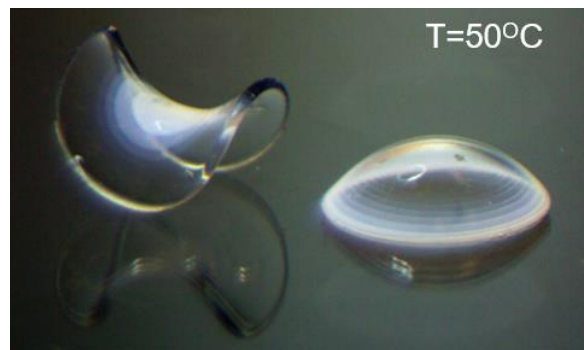
Figure 4-7 Pure polymer principle shapes at 50°C

Figure 4-8 Influence of parameters on accuracy

As expected when the area to thickness ratio decreases, it causes a decrease in accuracy. For samples with small area, pure bending configuration is not the minimum energy state and they still contain some stretching energy. Thus, at similar thickness, small samples cannot attain pure bending configuration.
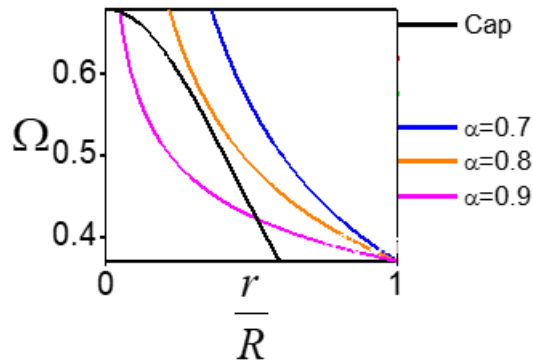
Figure 4-9 Relation of deswelling ratio and radius for cap and cones
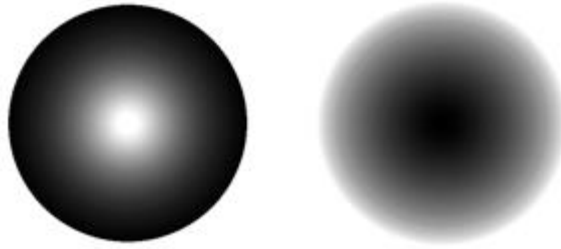
Figure 4-10 Grayscale exposure patterns for Cap and Saddle

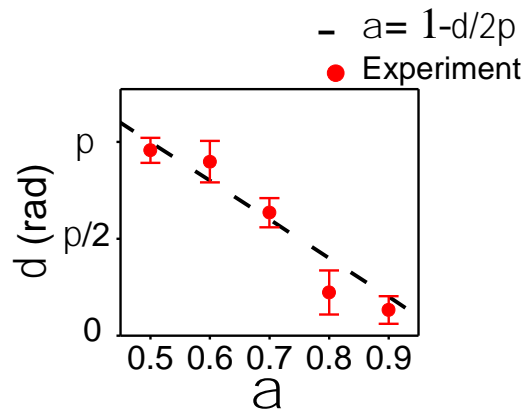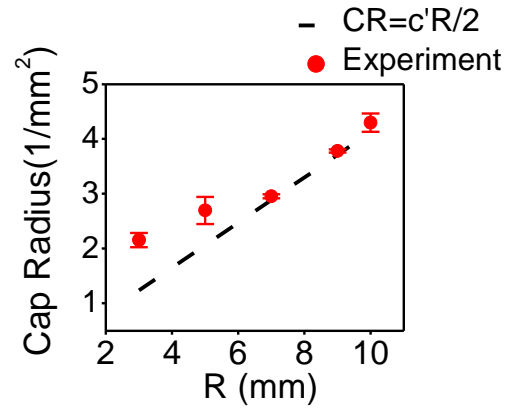Samples with sharp slope change in Ω need more number of grayscale levels to appropriately cover the changes of Ω. Therefore, the samples with more uniform Ω slopes, e.g., cones with lower α, show better accuracy.

As the sample temperature increases slightly over the LCST, the sample starts changing shape due to self-forming properties and transforms to the programmed shape over a short duration of time. This can be shown with a series of images of the sample taken during the sample goes slightly above transition temperature.

Figure 4-11 Heating the sample slightly over the transition temperature leading to programmed shape

4.5.3 Drying

After printing the samples, an important step to obtain the dry nanocomposite is drying of the hydrogel. This is possible due to the unique chemistry of the polymeric system. A drying ramp in which a combination of heating in the water bath, then heating in oven and subjection to ion deswelling was seen to give the best dried shape.
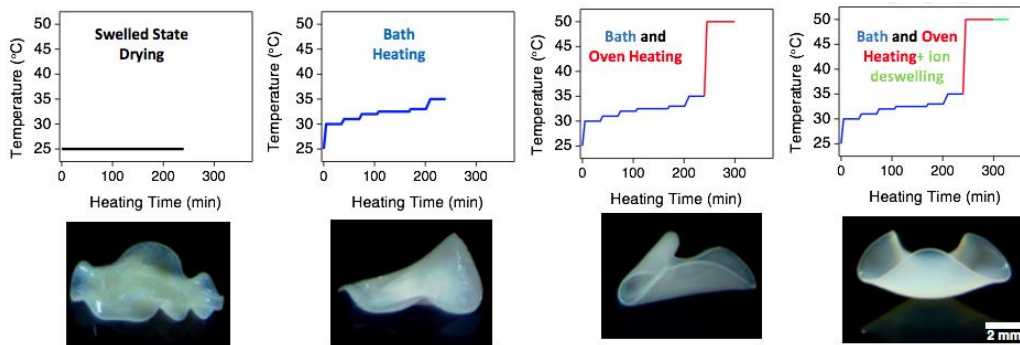
Figure 4-12 Drying ramps with final dried shapes

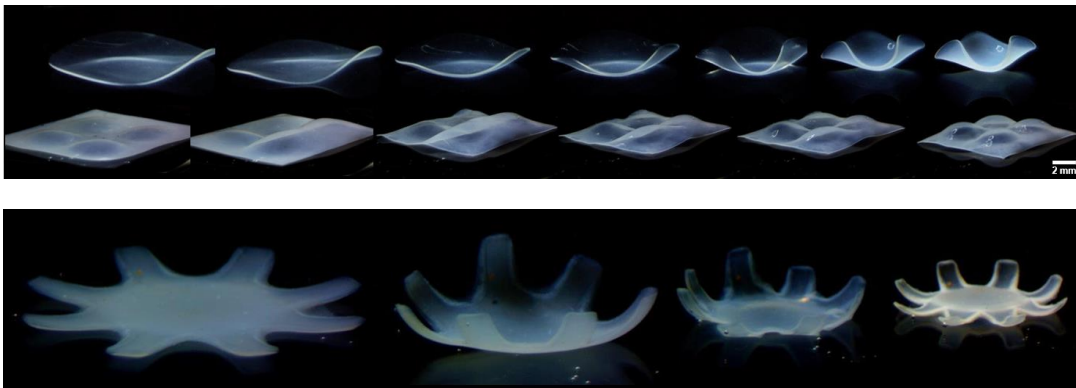After swelling for a day in water at 4^OC, the hydrogel samples were subjected to deswelling according to a temperature ramp over a period of 5 hours to allow sufficient time for the hydrogel to repel water. After heating up to a temperature of 35^OC in a water bath, the deswelled samples were transferred to an oven set at a temperature of 50^OC and left at the temperature for the samples to attain the set temperature. If the samples are exposed to ambient temperature just after they reach 35^OC, water present on the surface can deform the sample if the temperature of the water drops below the LCST. To avoid this, the samples were kept at 50^OC as described above and to help the samples maintain their shape; they were transferred to a near saturated ionic aqueous solution.[28] The previously fabricated samples were dried using the above method.
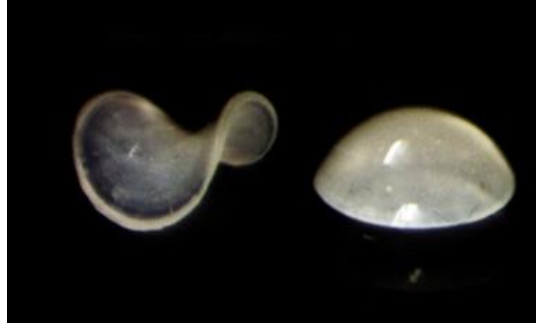
Figure 4-13 5% silica dried principle shapes
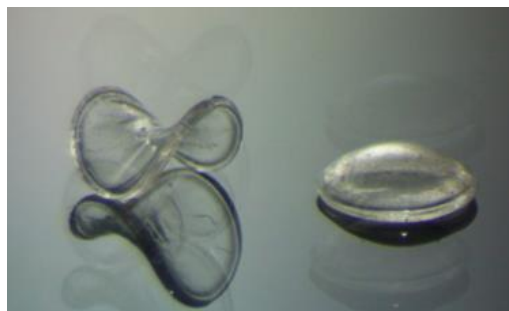
Figure 4-14 Pure polymer dried principle shapes

4.5.4 Surface study

In conventional techniques of 3D printing technologies, the printed objects show signs of imperfection caused during fabrication steps due to their layer-by-layer type of process. These are particularly evident for surfaces with curvatures in objects where the layer thickness is high. The layer edges are seen for these objects but due to the unique nature of our fabrication method, these curvatures are free of these imperfections that can be seen in the SEM images below.
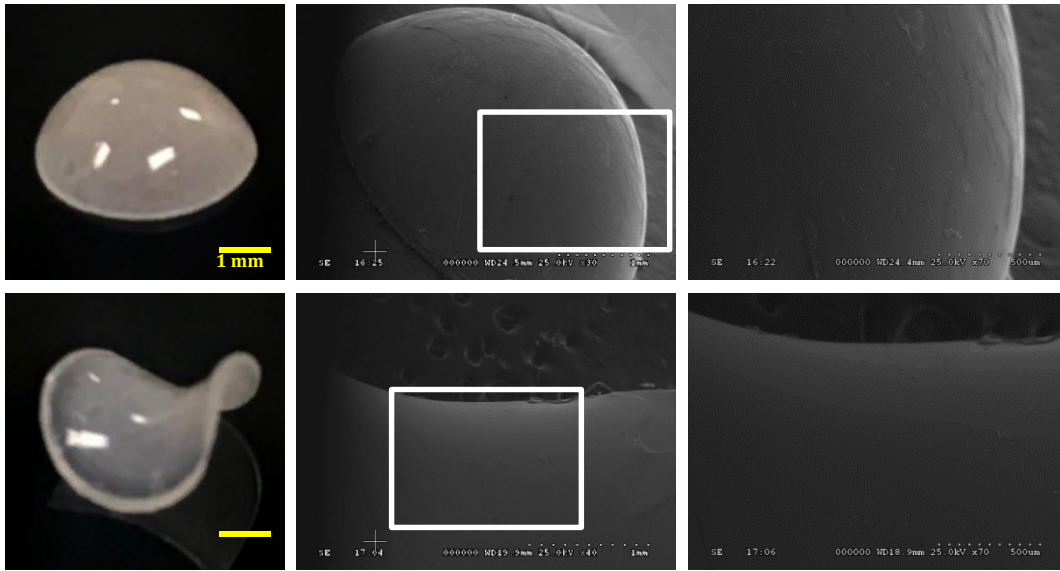
Figure 4-15 SEM images showing good non-processed surface finish for Cap and Saddle shapes

4.5.5 Mechanical test

Mechanical tests were carried out on the samples to obtain Hardness and yield strength of the nanocomposites. The tests were carried using a Vickers hardness tester with a four-sided pyramid tip. The tests are summarized below.
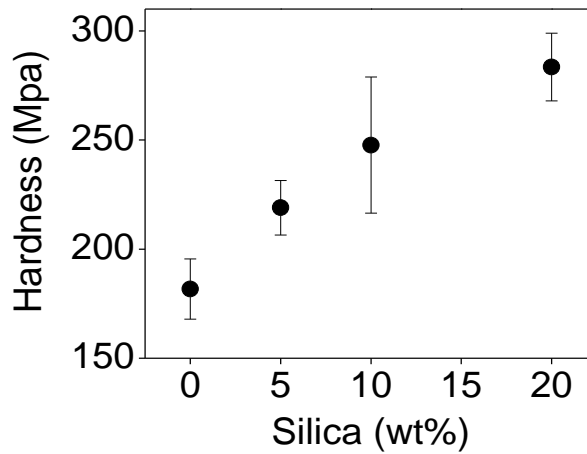
Figure 4-16 Hardness test for Silica nanocomposites with 0%, 5%, 10% and 20% solid loading

Table 4-2 Hardness values for polymers used in 3D printing

Polymer	Hardness (MPa)
PVA	39.2
ABS	77
PLA	83
PC	127.2
Nylon 6	157.9
PS	167.5
PMMA	**187.1**
PAA	**244.8**

The hardness for shape made using only polymer precursor is higher than most of the popular polymers used with current 3D printers. Addition of ceramic nanopowders leads to an increase in the hardness value of the composite as seen from the graph.

Figure 4-17 Yield strength of Silica nanocomposites with 0%, 5%, 10% and 20% solid loading
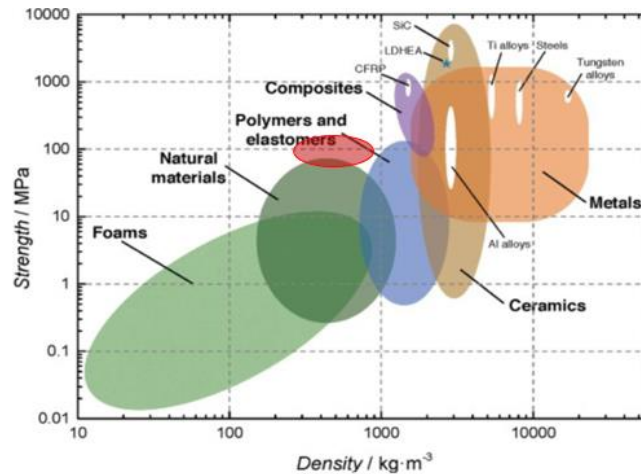
Figure 4-18 Ashby Chart for material selection[29]

When compared to pure polymer systems with similar density, the composites show better mechanical properties. Further processing like densification after polymer burnout is expected to increase this strength.

4.5.6 Processability

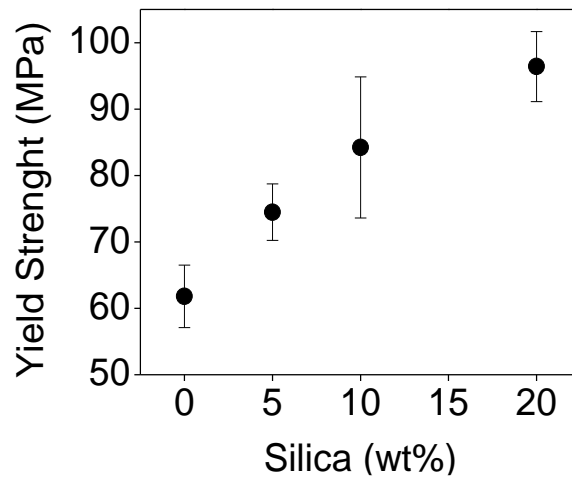An important factor when processing liquids is the viscosity. If the viscosity is high, flowability is low and the probability of air entrapment is high which can lead to various problems like lower than expected strength due to presence of weak points. If the viscosity is low enough, the solution can be spread properly over a surface or even tight areas where high viscosity liquids have a problem reaching. The viscosity of a solution increases if nanoparticles are introduced to the solution matrix, as the surface area to volume ratio of nanoparticles is quite large. In our experiments, we have a solid loading of up to 20% by weight that would have increased the viscosity but due to the use of solvents like water and acetone, the viscosity increase is limited. Moreover, after the printing of samples and deswelling, the dried samples are devoid of any solvents, which effectively provides a higher solid loading. For initial solid loading of 5%, 10% and 20% by weight, the final solid loading is calculated to be around 14.75%, 25.71% and 40.9% by weight respectively. This provides an important advantage in terms of processability for projection based additive

manufacturing as otherwise non-newtonian behavior of high solid loading dominates and become unusable.

4.5.7 Customizability

The polymer precursor we use can accommodate various nanoparticles which allows for tuning the properties of the 3D object. We have experimented with using zirconia and gold nanoparticles to show this ability of the system.

Figure 4-19 Gold and Zirconia nanocomposites
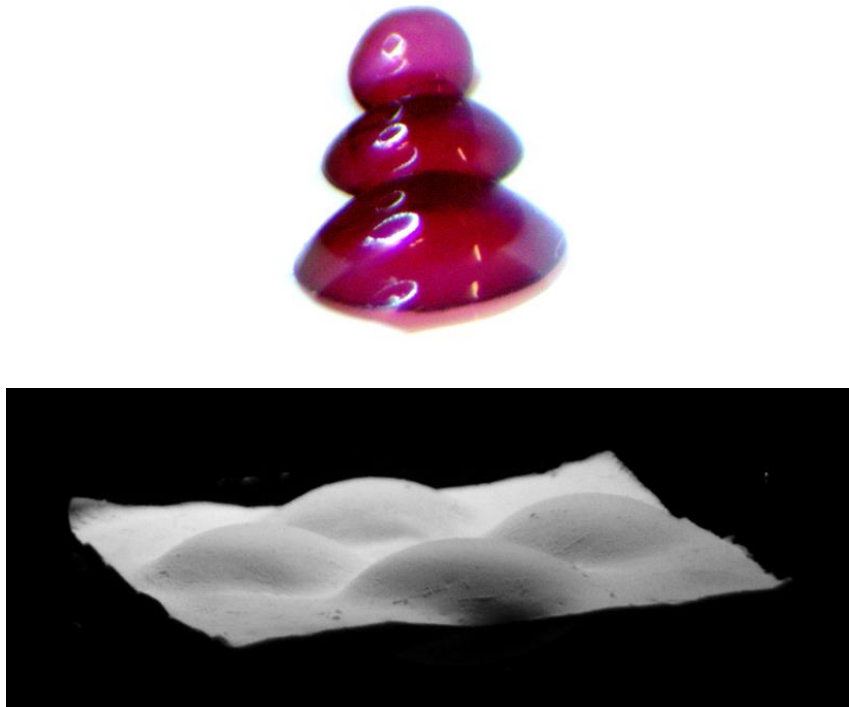
In addition to being able to customize the precursor, the number of precursors being used for printing an object can also be customized. Certain parts of the object can be made using a specific precursors giving complete control over the manufacturing process. This is demonstrated by printing and drying a cap and a saddle shape having patches of lines made of gold precursor.
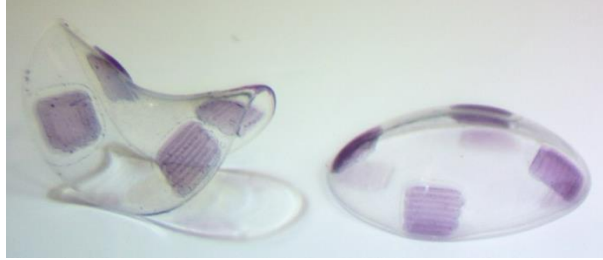
Figure 4-20 Cap and Saddle shapes with lines made of gold nanoparticle precursor

4.5.8 Scalability

The system is capable of printing shapes of any size less than the printing area in the same time regardless of the final size or shape. This is possible because of the this is a one step process and the shape is programmed instantaneously on a flat sheet instead of building it up layer-by-layer. Therefore, as long as size of the sheet is within the build area of the printer, any final shape and size object can be programmed. This is shown by printing and drying two identical shapes having different sizes simultaneously. The coin is used for scale reference.
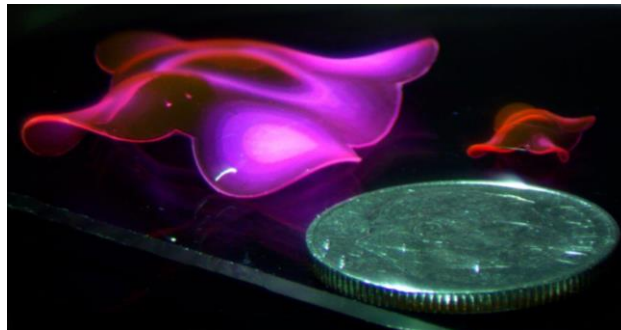
Figure 4-21 Two identical shapes printed and dried simultaneously

These experiments have supported to achieve the objectives of the study one of which was to study the effect of exposure time on the deswelling of the fabricated flat sheets. Printing a 2D shape takes much lower time, less than a minute while direct fabrication of a 3D object takes more than minutes and even hours to complete. Due to the nature of the exposure pattern system used, the same time is required for printing small as well as large

48

samples and hence provides excellent scalability. The ability to transform into 3D from 2D successfully eliminated the need for supports while the shrinkage of the sample due to deswelling contributed to the good non-processed surface finish as seen from the SEM images.

Chapter 5

Discussion

Conventional 3D printing is a cost-effective technique for fabricating 3D objects. The selection of materials available for use today has made the use of this technique valuable to almost all industries and a popular research topic for scientists. But even though now out of its infancy stage, several problems plague the widespread adoption of 3D printing machines. These include the need for long fabrication times due to the process of building layer upon layer to obtain the 3D object and the difficulty of scalability. Moreover, the fabricated objects contain surface imperfections or layer edges which sometimes ruin the aesthetic of the object. In addition to this, if the object has overhanging structures, then supports are needed to be printed which lead to material wastage and more importantly require additional time to print. Sheet forming is a technique which is scalable which means that the same object can be formed simultaneously in a single step. It also allows for single step fabrication which eliminates the need for layer-by-layer mechanism used in 3D printing. These inefficiencies were addressed in this study which used a thermosensitive polymer along with crosslinkers and a photoinitiator to form 2D hydrogels which have the ability to swell in aqueous medium. We used precursors with dispersed nanoparticles to obtain solid nanocomposites which are stable in air which are stable below the LCST of PNIPAm. Desirable surface finish and mechanical properties were shown during testing.

This process can be scaled up to print objects which are multiple times bigger than what is possible now with the use of advanced projector systems capable of projecting images without distortion. Additional material nanoparticles could be used to fabricate nanocomposites which could lead to better mechanical properties. Functional nanocomposites could also be fabricated to make sensors, actuators and transducers. Magnetic nanoparticles could be embedded to make the nanocomposite sensitive to magnetic fields. Use of metal nanoparticles would be useful for making nanocomposites

having a metallic properties and further processing could lead to smooth, pure metal parts without the need of post-processing.

Our nanocomposites were made of ceramic powders and the polymeric system which binds together the composite and provides the shape. If the polymer system is gradually removed in such a way as to fuse the nanoparticles together, a shape made of pure ceramic material could be obtained. This could then be sintered to fully fuse the nanoparticles together and if it is a silica shape, transparent glass shape can be obtained as the final product. We have also performed experiments in which we determined a suitable temperature ramp for the polymer system burnout. We introduce the nanocomposites to a furnace and use a predetermined temperature ramp to systematically eliminate all the components of the nanocomposite except the nanoparticles. This is done by gradual heating and strategic dwell times at specific temperatures.

Having achieved the objectives stated at the beginning of the previous chapter, work should be done to acquire more data regarding the further processing of the solid shapes.

Chapter 6

Conclusion

In this study, we looked at the effect of ceramic nanoparticle loading on the deswelling ratio at increasing light exposure. It was found that the deswelling ratio attains a plateau at higher exposures. We then showed an effective technique of drying deswelled hydrogels which retain their shape in air. The shapes were further studied by comparing with pure polymer precursors and their surface properties along with mechanical properties were analyzed. It was seen that the mechanical properties increase with an increase in the solid loading but the deswelling range decreases which restricts the range of shapes which can be fabricated using precursors with high solid loading. Finally, properties like customizability and scalability were demonstrated by using zirconia and gold nanoparticles in addition to silica nanoparticles and printing identical shapes with different sizes simultaneously.

References

[1] Egan, Paul F., Stephen J. Ferguson, and Kristina Shea. "Design of Hierarchical Three-Dimensional Printed Scaffolds Considering Mechanical and Biological Factors for Bone Tissue Engineering." *Journal of Mechanical Design* 139.6 (2017): 061401.

[2] https://www.ge.com/reports/printing-heads-3d-printing-launched-new-era-aircraft-design/

[3] https://wohlersassociates.com/blog/2016/01/popularity-of-fdm/

[4] Murphy, Edward J., Robert E. Ansel, and John J. Krajewski. "Method of forming a three-dimensional object by stereolithography and composition therefore." U.S. Patent No. 4,942,001. 17 Jul. 1990.

[5] Coats, Alma L., et al. "Stereolithography resins and methods." U.S. Patent No. 7,211,368. 1 May 2007.

[6] https://commons.wikimedia.org/wiki/File:Selective_laser_sintering_principle.png

[7] http://www.airbus.com/newsroom/news/en/2016/03/digital-materials.html

[8] http://www.abnewswire.com/pressreleases/4d-printing-market-trends-analysis-and-foresight-report-on-emerging-technologies-opportunities-sales-supply-demand-and-analysis-by-forecast-to-2022_191843.html

[9] https://www.marketsandmarkets.com/PressReleases/4d-printing.asp

[10] https://www.marketsandmarkets.com/PressReleases/4d-printing.asp

[11] https://www.grandviewresearch.com/industry-analysis/4d-printing-market

[12] Naficy, Sina, et al. "4D printing of reversible shape morphing hydrogel structures." *Macromolecular Materials and Engineering* 302.1 (2017).

[13] Ding, Zhen, et al. "4D rods: 3D structures via programmable 1D composite rods." *Materials & Design* 137 (2018): 256-265.

[14] Wei, Hongqiu, et al. "Direct-write fabrication of 4D active shape-changing structures based on a shape memory polymer and its nanocomposite." *ACS applied materials & interfaces*9.1 (2016): 876-883.

[15] Gladman, A. Sydney, et al. "Biomimetic 4D printing." *Nature materials* 15.4 (2016): 413.

[16] Huang, Limei, et al. "Ultrafast digital printing toward 4D shape changing materials." *Advanced Materials* 29.7 (2017).

[17] Lee, Jin Woo, In Hwan Lee, and Dong-Woo Cho. "Development of micro-stereolithography technology using metal powder." *Microelectronic engineering* 83.4-9 (2006): 1253-1256.

[18] Bartolo, P. J., and J. Gaspar. "Metal filled resin for stereolithography metal part." *CIRP Annals-Manufacturing Technology* 57.1 (2008): 235-238.

[19] Nguyen, Du T., et al. "3D-Printed Transparent Glass." *Advanced Materials* 29.26 (2017).

[20] Kotz, Frederik, et al. "Three-dimensional printing of transparent fused silica glass." *Nature* 544.7650 (2017): 337.

[21] Hu, Jack, Zdzislaw Marciniak, and John Duncan, eds. *Mechanics of sheet metal forming*. Elsevier, 2002.

[22] Hattalli, Vinod Laxman, and Shivashankar R. Srivatsa. "Sheet Metal Forming Processes–Recent Technological Advances." *Materials Today: Proceedings* 5.1 (2018): 2564-2574.

[23] http://brickisland.net/cs177/?p=144

[24] Gandhi, Arijit, et al. "Studies on thermoresponsive polymers: Phase behaviour, drug delivery and biomedical applications." *asian journal of pharmaceutical sciences* 10.2 (2015): 99-107.

[25] Sharon, Eran, and Efi Efrati. "The mechanics of non-Euclidean plates." *Soft Matter* 6.22 (2010): 5693-5704.

[26] Efrati, Efi, et al. "Spontaneous buckling of elastic sheets with a prescribed non-Euclidean metric." *Physica D: Nonlinear Phenomena* 235.1-2 (2007): 29-32.

[27] Efrati, Efi, et al. "Spontaneous buckling of elastic sheets with a prescribed non-Euclidean metric." *Physica D: Nonlinear Phenomena* 235.1-2 (2007): 29-32.

[28] Qiu, Yong, and Kinam Park. "Environment-sensitive hydrogels for drug delivery." *Advanced drug delivery reviews* 53.3 (2001): 321-339.

[29] Youssef, Khaled M., et al. "A novel low-density, high-hardness, high-entropy alloy with close-packed single-phase nanocrystalline structures." *Materials Research Letters* 3.2 (2015): 95-99.